Space Vector PWM Technique for a Three-level Asymmetrical Six-phase Drive

E. A. R. Engku Ariff, O. Dordevic, M. Jones, E. Levi
Faculty of Engineering and Technology
Liverpool John Moores University
Liverpool L3 3AF, U.K.

***Abstract*–A space vector pulse-width modulation (SVPWM) strategy for a three-level asymmetrical six-phase drive, with a single neutral point, based on vector space decomposition (VSD) approach is presented for the first time in this paper. The selection process, related to the determination of the right switching sequences for the proposed modulation strategy, is discussed in detail. The developed SVPWM strategy is then simulated in PLECS simulation package, while driving an asymmetrical six-phase induction machine running at no load. Obtained results prove the validity of the algorithm.**

***Keywords*–Multilevel inverters, multiphase drives, asymmetrical six-phase machine, space vector PWM.**

I. Introduction

The advantages offered by multiphase drives, compared to a conventional three-phase drive, are at this point in time well-known and understood. However, in recent years the research developments in the area of multiphase drives have accelerated significantly [1], with more and more attention devoted to multiphase drives with multiple three-phase stator winding sets. The main advantage of a multiphase drive is that it offers greater fault tolerance capabilities compared to the conventional three-phase drives. If a fault takes place in one of the three-phase machine's stator windings, the machine is not able to properly operate any more without additional hardware components. Yet, this is not the case in multiphase machines, as investigated in [2] for six-phase drives.

In addition, if an inverter is used for driving a multiphase machine, the current flowing from the dc-bus can be shared between more machine phases, thus offering possibility to use power semiconductors of lower rating in the design of the inverter. The inverter topology is not restricted to the two-level structure. Multilevel, e.g. three-level, inverter can also be used to drive the multiphase machine. The most common three-level topology is neutral-point-clamped (NPC) topology, which has been used for multiphase drives [3-6]. As the number of inverter's output leg voltage levels and the number of machine's phases increase, the complexity of developing a proper SVPWM will also increase.

The SVPWM technique, based on VSD approach introduced in [7], has been successfully developed for three-level five-phase (i.e. multilevel multiphase) drive for the first time in [3]. This modulation technique is then modified further and compared with carrier-based modulation strategies in [4]. Furthermore, the optimised steps of developing SVPWM algorithm presented in [4] are also adapted and applied for multilevel symmetrical six-phase and seven-phase drives in [5] and [6], respectively. This paper, for the first time, introduces a SVPWM strategy for a three-level asymmetrical six-phase drive based on the VSD approach.

II. Space Vector Algorithm

The topology of the three-level inverter fed asymmetrical six-phase machine, with single isolated neutral point, is shown in Fig. 1. The relationship between the machine phase voltages v_{phk} and inverter output leg voltages v_{LEGk} is:

$$v_{phk} = v_{LEGk} - \frac{1}{6}\sum_{k=1}^{6} v_{LEGk} \qquad (1)$$

where k = 1 to 6, which also corresponds to phases *a* to *f*. The second term in (1) represents common mode voltage, CMV. The desired output phase voltages are in a form of sinusoidal waveforms when the machine has sinusoidally distributed windings, as assumed here.

There are four possible combinations of switches per inverter leg, which lead to four possible inverter leg voltage (v_{LEGk}) levels, i.e. 0, $V_{dc}/2$, V_{dc} and high impedance output, when referred to the dc-bus negative rail, N_{dc}. However, the high impedance output is not considered in the space vector algorithm. By normalising the remaining inverter v_{LEGk} levels with $V_{dc}/2$, they are further denoted as 0, 1 and 2, respectively. Therefore, with respect to the analysed inverter, there are 3^6 = 729 possible switching states (denoted as 0 to 728) and $3^6 - 2^6$ = 665 phase voltage space vectors [8]. Note that the switching states (0 to 728) can also be represented in six-digit ternary

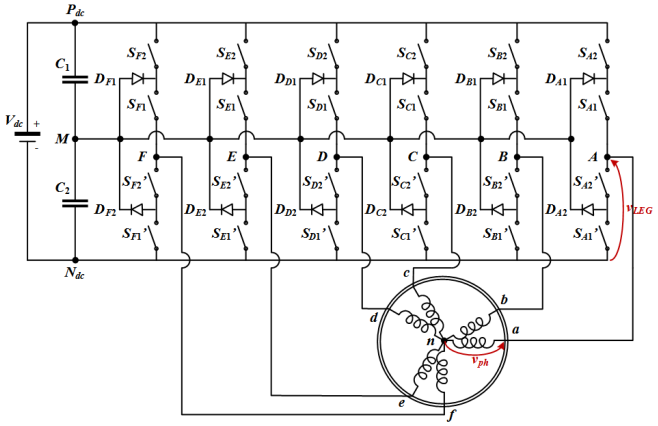

Fig. 1. Circuit topology of analysed three-level asymmetrical six-phase drive.

numeral system if normalised inverter leg voltage levels are used (000000 to 222222).

A. Three-level Asymmetrical Six-phase Inverter Space Vectors

The space vector projections of any set of asymmetrical six-phase variables (e.g. v_{phk} or v_{LEGk}) can be obtained by means of the transformation matrix:

$$\begin{bmatrix} v_\alpha \\ v_\beta \\ v_x \\ v_y \\ v_0 \end{bmatrix} = \frac{2}{6} \cdot \begin{bmatrix} 1 & \cos(\alpha) & \cos(4\alpha) & \cos(5\alpha) & \cos(8\alpha) & \cos(9\alpha) \\ 0 & \sin(\alpha) & \sin(4\alpha) & \sin(5\alpha) & \sin(8\alpha) & \sin(9\alpha) \\ 1 & \cos(5\alpha) & \cos(8\alpha) & \cos(\alpha) & \cos(4\alpha) & \cos(9\alpha) \\ 0 & \sin(5\alpha) & \sin(8\alpha) & \sin(\alpha) & \sin(4\alpha) & \sin(9\alpha) \\ 1/\sqrt{2} & -1/\sqrt{2} & 1/\sqrt{2} & -1/\sqrt{2} & 1/\sqrt{2} & -1/\sqrt{2} \end{bmatrix} \cdot \begin{bmatrix} v_a \\ v_b \\ v_c \\ v_d \\ v_e \\ v_f \end{bmatrix} \quad (2)$$

which is based on the VSD approach [7], where $\alpha = \pi/6$. Note that the transformation matrix above differs from the one normally used for an asymmetrical six-phase system, since only five variables result. The last row in (2) represents simultaneously a combination of the two zero-sequence components, with an appropriate scaling. This change has been found to be necessary because of the dwell time calculation described in sub-section II-D.

By substituting the leg voltages v_{LEGk} into (2), the projections of all 729 leg voltage space vectors into the two planes and the zero-sequence can be obtained. Similarly, projections of phase voltage v_{phk} space vectors can be obtained by substituting (1) into (2). One finds that the projections of v_{LEG} and v_{ph} space vectors onto α-β and x-y planes as well as onto 0 axis are identical. This means that determination of the switching sequences through selection of the leg voltage space vectors will also achieve the realisation of sinusoidal phase voltage waveforms. Furthermore, it can be shown that the phase voltage low order harmonics of the order $12k \pm 1$ (k = 0, 1, 2, 3…) are mapped into α-β plane. This plane in essence contributes to the machine torque/flux production, including torque ripple. On the other hand, the low order harmonics of the order $12k \pm 5$ (k = 0, 1, 2, 3…) and $3k$ (k = 1, 3, 5…) are mapped onto x-y plane and 0 axis respectively, [7]. These low order harmonics contribute to the machine losses and their existence is undesirable. In other words, the average values in the x-y plane and 0 axis must be controlled to zero.

B. Reduction of the Number of Switching States

Because of the huge number of switching states (729 for the analysed inverter topology), a method of eliminating the switching states that are of no use, known as order-per-sector law [3], is implemented first. This law requires that the projected switching states in each sector in α-β plane must follow the order of the reference phase voltage waveforms v^*_{phk} for the corresponding sector in the time domain. The v^*_{phk} waveforms can be defined as:

$$v^*_{phk} = V^* \cos(\omega t - i \cdot \pi/6) \quad (3)$$

where V^* is the reference peak value and k = 1 to 6, which also corresponds to phases a to f while the corresponding values of i are i = 0, 1, 4, 5, 8 and 9. By plotting reference phase voltages of (3), one finds that v^*_{phk} change their mutual order at 0°, 15°, 30°, 60° 75°, 90°, 120°, etc. These angles also correspond to the sector angles in α-β plane where the odd sectors are further sub-divided into two sections at 15° angle, while even sectors span entire 30°. For example, within the first 15° the order of v^*_{phk} is: $v^*_a \geq v^*_b \geq v^*_f \geq v^*_c \geq v^*_e \geq v^*_d$. According to the order-per-sector law, the switching states of all space vectors whose projections fall within first 15° of the α-β plane, should follow the same order as v^*_{phk}. Taking as an example switching state 651 (i.e. 220010), one can see that its α-β projection is located within first 15° sector, but it does not satisfy the required order because $v_C < v_E$. Hence this switching state (and many others) can be eliminated. As a result, the number of switching states is significantly reduced, from 729 to 195. These remaining switching states and their corresponding space vector projections into α-β and x-y planes, as well as 0 axis, are shown in Fig. 2. The space vectors in Fig. 2 are labelled in decimal representation; conversion to ternary representation should be done if interpretation of each state of the inverter legs is desired.

C. Determination of Potential Switching Sequences

Determination of the potential switching sequences starts with identifying the potential starting switching states, which are identified based on the composition of their state levels. For the analysed inverter, the composition of state levels of the potential starting switching states can be ‘zeros’, ‘ones’ or combination of the two [4]. This is so because it is desirable that the v_{LEGk} levels change by one level up per transition, during the first half of the switching period, and hence having level ‘two’ in the starting switching state would not allow any further increase in that leg. In this way, the symmetrical pattern will be obtained (all the legs will decrease for one level in the second half of the switching period) and the switching losses and dv/dt will be minimised. As a result, only 32 out of 195 remaining switching states (enclosed in the red boxes in Fig. 2a) meet the stated requirements and can be chosen as starting switching states.

Once the starting switching state is selected, the other subsequent switching states in the potential switching sequence can be determined next. Usually, these subsequent switching states can be easily determined since they are projected in the same sector as the projection of starting switching state in the α-β plane [4-6, 9]. However, for asymmetrical six-phase case, this is not applicable. Therefore, all remaining switching states should be considered as candidates for the subsequent switching states in each respective potential switching sequence.

There are six transitions of v_{LEGk} levels (only the first half of switching period is considered since the transitions of v_{LEGk} levels are reversed in the other half) in one switching sequence. Hence, there are 6! = 720 possible permutations of switching sequences per each starting switching state (e.g. the transition may happen in the 1st leg first, then in the 2nd, 3rd, 4th, 5th and 6th leg, or in any other permutation order). However, not all possible permutations of switching sequences can be considered as potential switching sequences, since some of the possible permutations include switching states which have been previously eliminated by the order-per-sector law. Therefore, the number of potential switching sequences

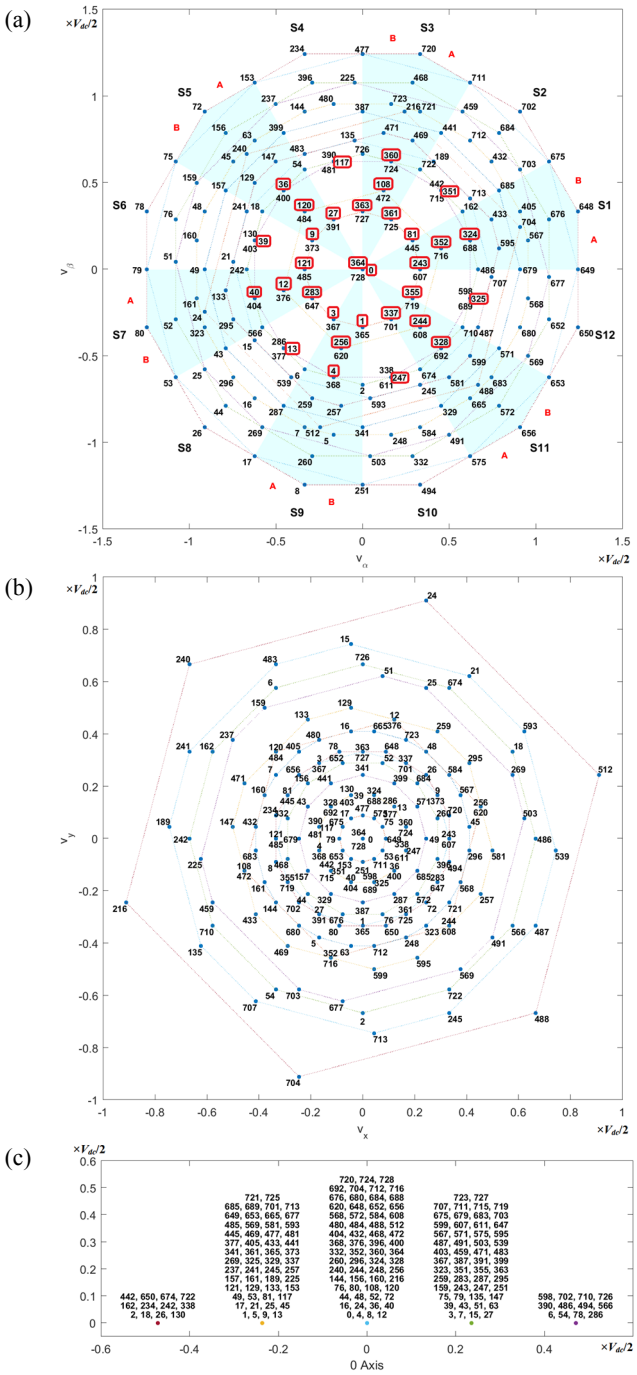

Fig. 2. Projection of phase voltage space vectors of the analysed inverter after implementation of the order-per-sector law in the: (a) α-β plane, (b) x-y plane and (c) 0 axis.

from the possible permutations should be less than 720 per starting switching state. The problem contains too many switching states and too many switching sequences to be considered analytically. Therefore, the problem was solved by using Matlab code.

As an example, for starting switching state 324 (i.e. 110000), only 102 out of 720 permutations of switching sequences can be considered as actual potential switching sequences. The possible single level transitions of v_{LEGk} of those 102 potential switching sequences are illustrated with six

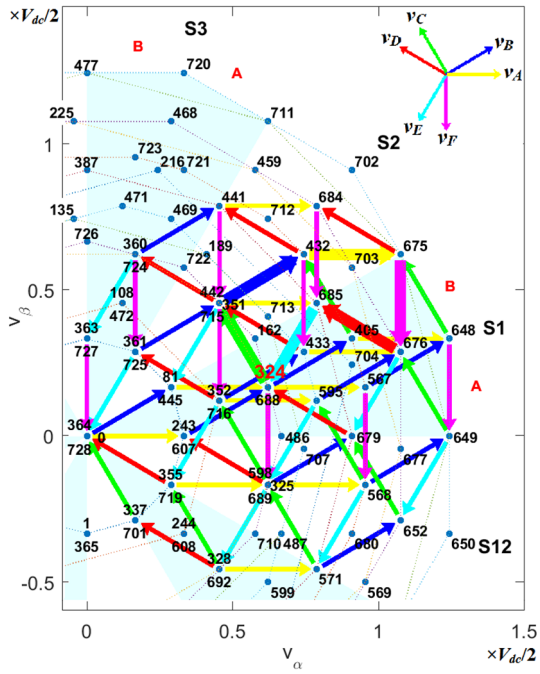

Fig. 3. All possible single level increasing transitions of v_{LEGk} for starting switching state 324 (110000).

different colours of arrows in Fig. 3 (only transitions in α-β plane are shown). This figure corresponds to the figure generated by Matlab code: visual determination of all 102 six-angled patterns is still possible, but would be very tedious. Hence, the problem was solved by Matlab code. Also, note that the transition patterns in α-β and x-y planes as well as 0 axis of these 102 potential switching sequences are different from each other. Although there are seven switching states per switching sequence, the first and the last switching state project into identical space vector and a switching sequence contains only six space vectors, which agrees with [10].

Since this permutation method determines the potential switching sequences by taking into account all possible single level increasing transitions of v_{LEGk} for each identified starting switching state, this method is also valid for other drives with any number of inverter levels and machine phases.

D. Dwell time Calculation and Sector Division

The calculation of dwell times is based on space vector projections of potential switching sequences. In other words, each transition pattern yields different values of dwell times and, naturally, potential switching sequences which correspond to the same transition patterns will have the same values of dwell times [6]. The dwell times can be calculated using the volt-second balancing principle and time balancing equations (T_s stands for the switching period):

$$\begin{bmatrix} T_1 \\ T_2 \\ T_3 \\ T_4 \\ T_5 \\ T_6 \end{bmatrix} = \begin{bmatrix} v_{\alpha,1} & v_{\alpha,2} & v_{\alpha,3} & v_{\alpha,4} & v_{\alpha,5} & v_{\alpha,6} \\ v_{\beta,1} & v_{\beta,2} & v_{\beta,3} & v_{\beta,4} & v_{\beta,5} & v_{\beta,6} \\ v_{x,1} & v_{x,2} & v_{x,3} & v_{x,4} & v_{x,5} & v_{x,6} \\ v_{y,1} & v_{y,2} & v_{y,3} & v_{y,4} & v_{y,5} & v_{y,6} \\ v_{0,1} & v_{0,2} & v_{0,3} & v_{0,4} & v_{0,5} & v_{0,6} \\ 1 & 1 & 1 & 1 & 1 & 1 \end{bmatrix}^{-1} \cdot \begin{bmatrix} v_\alpha^* \\ v_\beta^* \\ v_x^* \\ v_y^* \\ v_0^* \\ 1 \end{bmatrix} \cdot T_s \tag{4}$$

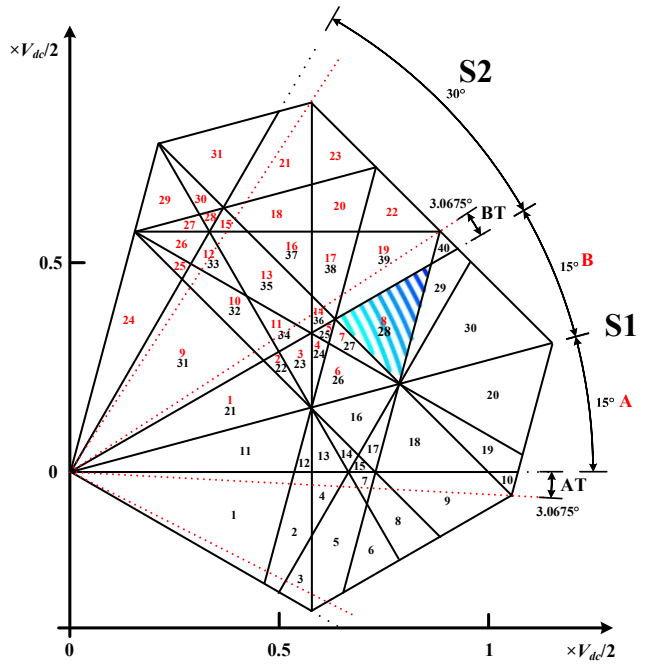

Fig. 4. Regions of application for all possible transition patterns of starting switching states 324 and 351 (region of application for transition patterns denoted by large arrows in Fig. 3 is plotted by dots using Matlab).

The first five rows of the inverse matrix in (4) correspond to α, β, x, y and 0 projections of any chosen switching sequence. The last row corresponds to the time balancing equation which ensures that the sum of calculated dwell times is equal to T_s. The reference voltages of α and β axes in (4), i.e. v_α^* and v_β^*, are set to $V^*\cdot\cos(\omega t)$ and $V^*\cdot\sin(\omega t)$, respectively, which corresponds to sinusoidal references of (3). As previously mentioned, in order to obtain sinusoidal v_{phk} waveforms, the x, y and 0 axes components must be controlled and set to zero. Therefore, the references for other axes, i.e. v_x^*, v_y^* and v_0^*, are set to zero.

Yet, the solutions of dwell time calculation of each transition pattern only exist in certain regions in α-β plane, known as regions of application. These regions can be identified using visualisation of numerical solutions (calculated using Matlab programme) in α-β plane [6]. As an example, switching sequence 110000-111000-121000-221000-221001-221101-221111, which corresponds to the transition patterns denoted by thick arrows in Fig. 3, forms a region of application which is illustrated with coloured dots in Fig. 4. One can find that for the analysed starting switching state 324, i.e. 110000, out of 102 potential switching sequences, 40 have a solution of (4), and hence have a region of application as in Fig. 4. As an example, the regions of application of all transition patterns with starting switching states 324, i.e. 110000 (denoted by 1 to 40), and 351, i.e. 111000 (denoted by 1 to 31 in red), are also shown in Fig. 4. These regions of application divide the sectors into several geometrical shapes, hence they are also known as sub-sectors.

As can be seen in Fig. 4, some of the regions of application are applicable to both potential switching sequences with starting switching states 324 and 351. Since the existence of the region of application is unique for each transition pattern, this indicates that some potential switching sequences have the same transition patterns, thus causing redundancy in potential switching sequences.

E. Potential Switching Sequence Optimisation

Since there are redundancies in potential switching sequences, the next stage is the selection process of the right switching sequences, based on minimization of the switching losses. In other words, all switching sequences within the same sub-sector should have the same starting switching state, hence preventing additional switching losses during transition between sub-sectors [9]. However, in Fig. 4, sub-sectors 10 and 40 of the starting switching state 324 are located outside the first sector S1. Also, they do not have any other redundant potential switching sequences. Therefore, in order to meet the stated requirement, additional small sectors at each side of odd sectors, denoted by AT and BT, which consist of eight additional sub-sectors each, are introduced, as shown in Fig. 4. Hence, it can be said that an odd sector is comprised of A, AT, B and BT sectors. The selected switching sequences of S1-A are listed in Table I as an example, while the selected switching sequences of other sectors can be acquired in the same way. Note that only the switching states in the first half of the switching period are listed; the order of the switching states is reversed in the second half.

F. Sub-sector Determination

As the projected v_{ph}^* space vector is moving in circular manner in the α-β plane, it passes through the sectors as well as sub-sectors. Therefore, the corresponding switching sequences and calculated dwell times have to be applied accordingly. The present location of projected v_{ph}^* space vector and sub-sector in which it is situated can be determined by using the sub-sectors' borders as limits [3]. An illustration of how this method is applied for S1-A is shown in Fig. 5. There are nine borders in S1-A and these borders can be projected onto six perpendicular axes P_1 to P_6. The distances of intersection points between the projected borders and those axes with respect to origin (denoted as L_{11}, L_{21}, L_{22} … L_{61}) can be calculated using simple trigonometry, which gives $L_{11}= L_{31}= L_{41}= L_{61}= \sqrt{3}/6V_{dc}$, $L_{21}= L_{51}= \sqrt{2}(\sqrt{3}-1)/4V_{dc}$, $L_{22}= L_{52}= \sqrt{2}/4V_{dc}$ and finally $L_{23}= \sqrt{2}(\sqrt{3}-1)/2V_{dc}$. These four

TABLE I. SELECTED SWITCHING SEQUENCES FOR S1-A.

Sub-sector	Selected switching sequence
A	110000-110001-111001-111011-111111-211111-221111
B	110000-110001-111001-111011-211011-211111-221111
C	110000-110001-111001-111011-211011-221011-221111
D	110000-110001-111001-211001-211011-221011-221111
E	110000-110001-210001-211001-211011-221011-221111
F	110000-110001-111001-211001-221001-221011-221111
G	110000-110001-210001-211001-221001-221011-221111
H	110000-110001-210001-220001-221001-221011-221111
I	110000-210000-210001-220001-221001-221011-221111
J	110000-210000-220000-220001-221001-221011-221111

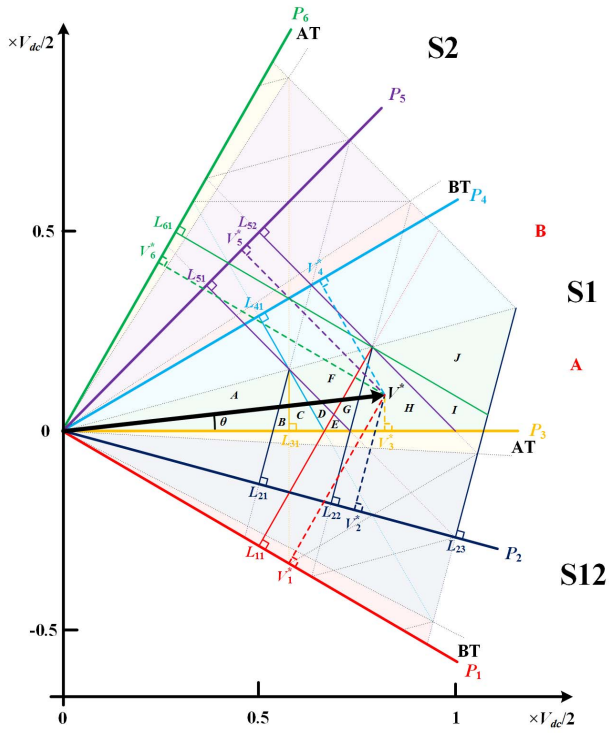

Fig. 5. Sub-sector determination based on the location of the projected v_{ph}^* space vector in S1-A.

limits are denoted further with L_1, L_2, L_3 and L_4, respectively.

In addition, the projected reference voltage (v_{ph}^*) space vector is also projected onto the same corresponding axes (denoted as V_1^* to V_6^*) and then compared to those limits. As a result, by applying this method, the exact location, i.e. the sub-sector where it is located, for the projected v_{ph}^* space vector at any given time can be determined. As an example, the required conditions in determining the sub-sectors in S1-A are listed in Table II.

III. Simulation Results

Despite the complex process presented in Section II, implementation of the proposed space vector algorithm is rather simple. The switching signals intended for the inverter's switches are generated based on the switching states within particular switching sequence corresponding to the present location (i.e. sub-sector) of the reference space vector. The duration for which each switching state should be applied is determined from the calculated dwell times. Therefore, only these three components (current sub-sector, corresponding switching sequence, and the dwell times) are essential for generating the switching signals. As shown in Section II, all sub-sectors' switching sequences can be determined offline. In addition, inverse matrices of (4), used for the dwell time calculation, can also be pre-calculated offline and stored in the memory for each sub-sector. Therefore, once all offline steps of Section II are completed, the final implementation is simple, and basically reduces to sub-sector determination (operations as in Table II), and fetching of the data (switching sequences and pre-calculated inverse matrices for dwell time calculation), from the memory. It is not necessary to store the

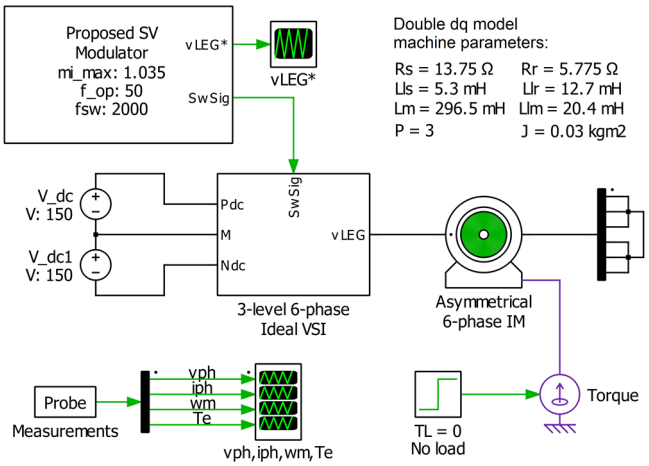

Fig. 6. Simulation diagram of the proposed space vector PWM for three-level asymmetrical six-phase drive, with machine parameters of [12].

TABLE II. Conditions Defining the Sub-sectors that Correspond to the Location of the v_{ph}^* Space Vector in S1-A.

Sub-sector	Conditions	
A	$V_2^* \le L_2$	where:
B	$V_2^* > L_2,\quad V_3^* \le L_3$	$V_1^* = V^*\cos(\omega t+\pi/6)$
C	$V_3^* > L_3,\quad V_4^* \le L_1$	$V_2^* = V^*\cos(\omega t+\pi/12)$
D	$V_4^* > L_1,\quad V_5^* \le L_2,\quad V_1^* \le L_1$	$V_3^* = V^*\cos(\omega t)$
E	$V_1^* > L_1,\quad V_5^* \le L_2$	$V_4^* = V^*\cos(\omega t-\pi/6)$
F	$V_5^* > L_2,\quad V_1^* \le L_1$	$V_5^* = V^*\cos(\omega t-\pi/4)$
G	$V_1^* > L_1,\quad V_5^* \le L_2,\quad V_2^* \le L_3$	$V_6^* = V^*\cos(\omega t-\pi/3)$
H	$V_2^* > L_3,\quad V_5^* \le L_2$	
I	$V_5^* > L_3,\quad V_6^* \le L_1,\quad V_2^* \le L_4$	
J	$V_6^* > L_1,\quad V_2^* \le L_4$	

data in the memory for all 12 sectors and their sub-sectors. By simple manipulations one can see that the data for other sectors can be obtained from the data for the first three sectors S1, S2 and S3; therefore, only the data for S1, S2 and S3, and their sub-sectors, should be stored in the memory.

A PWM modulator based on the proposed space vector algorithm is developed and simulated in PLECS software, as shown in Fig. 6. The inverter is taken as ideal and dc-bus voltage V_{dc} is 300 V. The algorithm is tested for full linear range of modulation index m_i, i.e. from 0.1 to 1.035, with 0.05 increment using *V/f* control (machine rated frequency is 50 Hz). The machine is controlled in open loop manner, it operates without load, and the switching frequency is 2 kHz. The maximum achievable m_i for the analysed topology is 1.035 [11]. The m_i is defined as:

$$m_i = V^* / (V_{dc}/2) \tag{5}$$

The performance of the algorithm for full linear rage of m_i is determined by using the calculated phase '*a*' voltage and current total harmonic distortions (THD) as figures of merit. The phase voltage and current THD are calculated as:

$$\mathrm{THD}_v = \sqrt{\sum_{h=2}^{H} V_h^2 / V_1^2} \qquad \mathrm{THD}_i = \sqrt{\sum_{h=2}^{H} I_h^2 / I_1^2} \tag{6}$$

where V_h and I_h represent the *h*-th harmonics of the voltage and current in the spectrum, while V_1 and I_1 are the fundamental values of phase voltage and current, respectively.

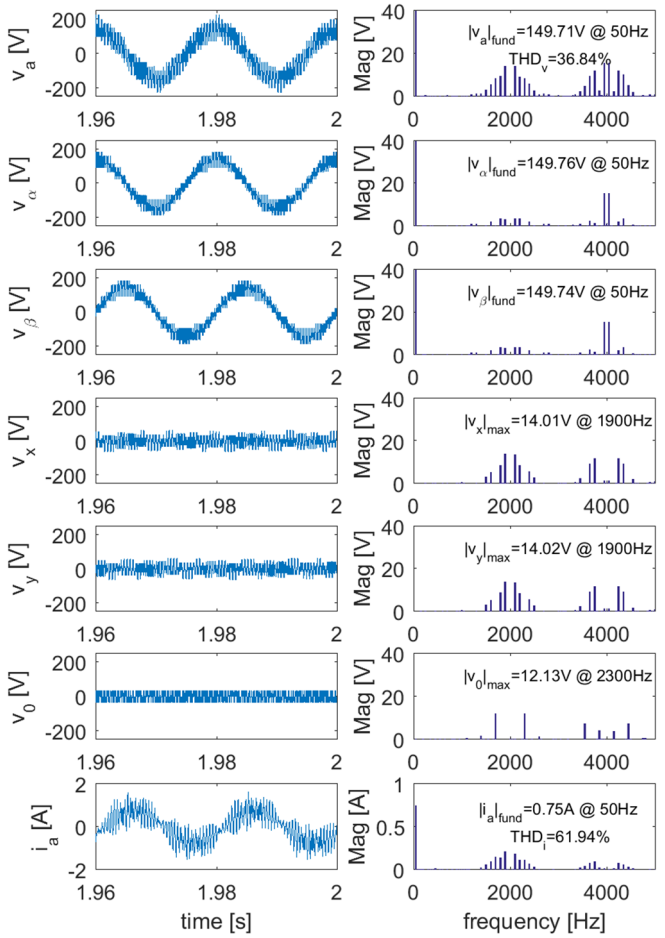

Fig. 7. Phase '*a*' voltage, phase voltage components (v_α, v_β, v_x, v_y and v_0), phase '*a*' current and their corresponding frequency spectra.

Harmonic components up to H = 420 (21 kHz), i.e. first ten sidebands, are used for THD calculation.

Simulation results when m_i = 1 are shown in Fig. 7. The fundamental magnitude of phase voltage waveform is 150 V, which is in agreement with (5). In addition, it can be seen that the low order harmonics of the order $12k \pm 5$ (k = 0, 1, 2, 3…) and $3k$ (k = 1, 3, 5…), which are mapped into x-y plane and onto 0 axis, respectively, do not exist in the phase voltage waveform frequency spectrum. This is expected since the x, y and 0 axis components are controlled to zero. This confirms the ability of the proposed algorithm to realise desired sinusoidal phase voltage waveforms without the existence of low order harmonics. The phase voltage THD$_v$ and THD$_i$ for full linear range of m_i are shown in Fig. 8.

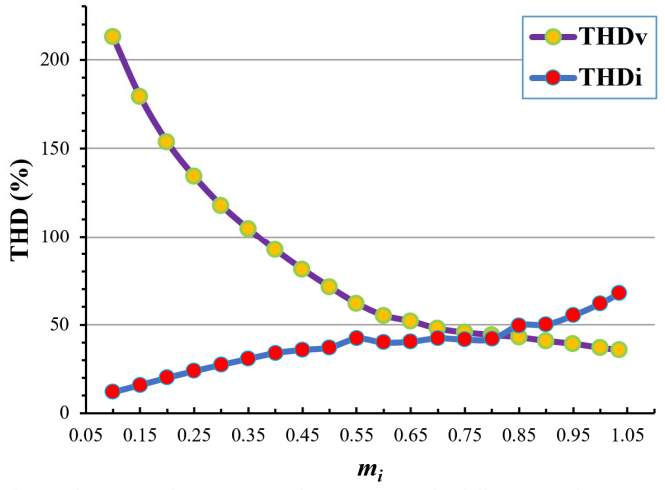

Fig. 8. Phase '*a*' voltage THD$_v$ and current THD$_i$ for full m_i range from 0.1 to 1.035.

IV. Conclusion

A space vector PWM algorithm for three-level asymmetrical six-phase drives, based on the VSD approach, is proposed for the first time. The paper shows offline steps and describes the process of switching sequence determination, how the sectors should be divided into sub-sectors, and how the dwell times can be calculated. Although the offline process is tedious, the practical implementation is simple.

The algorithm is developed and simulated in PLECS software, using an asymmetrical six-phase induction machine model and parameters, for the full linear range of the modulation index. The simulation results show that the required fundamental output voltage is achieved, and that the low order harmonics are not present in the output phase voltage and current, thus validating the developed space vector PWM algorithm.

References

[1] E. Levi, F. Barrero, and M. J. Duran, "Multiphase machines and drives - Revisited," *IEEE Trans. Ind. Electron.,* vol. 63, pp. 429-432, 2016.

[2] H. S. Che, M. J. Duran, E. Levi, M. Jones, H. Wooi-Ping, and N. Abd Rahim, "Postfault operation of an asymmetrical six-phase induction machine with single and two isolated neutral points," *IEEE Trans. Power Electron.,* vol. 29, pp. 5406-5416, 2014.

[3] L. Gao and J. E. Fletcher, "A space vector switching strategy for three-level five-phase inverter drives," *IEEE Trans. Ind. Electron.,* vol. 57, pp. 2332-2343, 2010.

[4] O. Dordevic, M. Jones, and E. Levi, "A comparison of carrier-based and space vector PWM techniques for three-level five-phase voltage source inverters," *IEEE Trans. Ind. Informatics,* vol. 9, pp. 609-619, May 2013.

[5] E. A. R. Engku Ariff, O. Dordevic, and M. Jones, "Space vector PWM technique for a three-level six-phase drive," in *Proc. 8th IET Int. Conf. Power Electron., Mach. and Drives PEMD*, Glasgow, UK, 2016, pp. 1-6.

[6] O. Dordevic, E. Levi, and M. Jones, "A vector space decomposition based space vector PWM algorithm for a three-level seven-phase voltage source inverter," *IEEE Trans. Power Electron.,* vol. 28, pp. 637-649, 2013.

[7] Y. Zhao and T. A. Lipo, "Space vector PWM control of dual three-phase induction machine using vector space decomposition," *IEEE Trans. Ind. Appl.,* vol. 31, pp. 1100-1109, 1995.

[8] O. Lopez, E. Levi, F. D. Freijedo, and J. Doval-Gandoy, "Number of switching state vectors and space vectors in multilevel multiphase converters," *Electron. Letters,* vol. 45, pp. 524-525, 2009.

[9] B. P. McGrath, D. G. Holmes, and T. A. Lipo, "Optimized space vector switching sequences for multilevel inverters," *IEEE Trans. Power Electron.,* vol. 18, pp. 1293-1301, 2003.

[10] J. W. Kelly, E. G. Strangas, and J. M. Miller, "Multiphase space vector pulse width modulation," *IEEE Trans. Energy Conv.,* vol. 18, pp. 259-264, 2003.

[11] D. Dujic, E. Levi, and M. Jones, "Dc bus utilisation in multiphase VSI supplied drives with a composite stator phase number," in *Proc. IEEE Int. Conf. Ind. Techn. ICIT*, Vina del Mar, Chile, 2010, pp. 1495-1500.

[12] H. S. Che, A. S. Abdel-Khalik, O. Dordevic, and E. Levi, "Parameter estimation of asymmetrical six-phase induction machines using modified standard tests," *IEEE Trans. Ind. Electron.*, vol. 64, no. 8, pp. 6075-6085, 2017.